Wetting Behavior and Functionality Restoration of Cold-Sprayed Aluminum-Quasicrystalline Composite Coatings

Reza Jafari[1] · Jarkko Kiilakoski[2] · Mari Honkanen[3] · Minnamari Vippola[1,3] · Heli Koivuluoto[1]

Abstract Coating design is an efficient strategy to engineer wettability of surfaces and adjustment of the functionality to the necessities in industrial sectors. The current study reveals the feasibility of functional aluminum/quasicrystalline (Al-QC) composite coatings fabrication by cold spray technology. A commercially available Al-based quasicrystalline powder (Al-Cr-Fe-Cu) was combined with aluminum alloy (Al6061) feedstock materials to make coatings with various compositions. A set of cold spray process parameters was employed to deposit composite coatings with different QC-Al ratios and Al6061 coatings as counterparts. The wettability of the coating surfaces was measured by static water droplet contact angles using a droplet shape analyzer and investigation of the dynamic of water droplet impact by high-speed imaging. Through microstructural studies, the Al-QC composites revealed dense structure, well-integrated and adherent deposits, providing structural reliability and enhanced hydrophobic behavior. In the last step of this work, composite coatings were deposited over eroded cold-sprayed Al6061 and a selected composite to demonstrate the feasibility of repairing the damaged part and function restoring. The results and approach used in this work provide understanding of cold-sprayed Al-QC composite coatings manufacturing and their wetting behavior state for cross-field applications.

Keywords aluminum alloy · cold spray · composite coating · quasicrystal · repairing · wettability

✉ Reza Jafari
reza.jafari@tuni.fi

Jarkko Kiilakoski
jarkko.kiilakoski@saint-gobain.com

Mari Honkanen
mari.honkanen@tuni.fi

Minnamari Vippola
minnamari.vippola@tuni.fi

Heli Koivuluoto
heli.koivuluoto@tuni.fi

1   Materials Science and Environmental Engineering Unit, Tampere University, Tampere, Finland

2   Saint-Gobain Coating Solutions, Avignon, France

3   Tampere Microscopy Center, Tampere, Finland

Introduction

In many industrial sections, operational challenges exist when a component is in contact with water in the working condition. Corrosion, fouling, current leakage and heat transfer efficiency reduction, to name a few, are examples

of such complications that can be avoided or reduced by employing hydrophobic coatings. By virtue of the low wetting feature, hydrophobic coatings can reduce water droplet contact and adhesion, interrupting unwanted interactions with water. Acknowledging immense potential applications, there has been an increasing interest in developing durable hydrophobic coatings in both academic and industrial fields (Ref [1, 2]).

Wetting behavior can be determined by measuring water droplet contact angle (CA), defined as the angle between the water–air interface tangent and the water–solid interface (Ref [3]). Surfaces with water droplet CAs of $90° < \Theta < 150°$ are considered hydrophobic, whereas higher and lower CAs might be classified in the categories of superhydrophobic and hydrophilic, respectively (Ref [4]). Developing testing equipment enabled scientists to enrich their understanding of wetting by obtaining supplementary data from non-static testing methods such as impacted droplet dynamics (Ref [5-7]). A droplet hitting the surface might show different modes of splashing, spreading or rebounding, depending on the properties of liquid, impact condition (e.g., Weber number, hitting angle) and surface properties (Ref [5]). In case of water-repellent surfaces, the impacted water droplets tend to bounce off from the surface and reduce their contact with the surface (Ref [5, 8]). This scientific knowledge has led to the technical ability to design surfaces with regulated wettability for cross-field applications such as drag reduction, anti-icing, self-cleaning, corrosion protection, heat transfer enhancement and electricity generation, to name a few (Ref [1, 9-14]). In general, surface chemistry modification and altering the surface roughness are effective strategies to fabricate water-repellant surfaces (Ref [1, 15-18]). However, the robustness of most effective candidates generally made through thin layer modification of surfaces, nanotextured surfaces, polymeric functionalization or fragile oxide layers is insufficient to fulfill the application-specific requirements, such as sufficient mechanical properties (Ref [19-21]). The types of structure that come out of nanoscale texturing and thin layer modifications are highly delicate and can be compromised during operation by environmental factors. In addition, mass production can be challenged by the facilities and process-scale constraints and cost-related issues (Ref [1, 2]). On the other hand, metals and metal alloys like Fe- and Al-based alloys as conventional materials in most structures and industrial sectors merely show hydrophilic behavior (Ref [22-24]). Therefore, facile generation of industry-scale and robust coatings with hydrophobic behavior is a pressing task.

Thermal spray technologies with extensive possibilities can deposit versatile coating materials from soft polymeric materials to hard, brittle ceramics that meet the demands of the industry (Ref [18, 25]). The efforts to fabricate non-wetting surfaces using thermal spray technologies consist of two main strategies: surface texturing and chemical modification of the surfaces (Ref [12, 26-32]). To name some examples, two-step modification of the surface by flame spraying of nano-Al_2O_3 (Ref [26]) or suspension plasma spraying of TiO_2 (Ref [27]) gave rise to water droplet CAs via producing a hierarchical roughness. Chemical modification of surface is followed in majority of wetting-engineered thermally sprayed coating. Controlled heat treatment of thermally sprayed coatings (Ref [28]), oil impregnation inside the structure (Ref [29]), modification of thermal spray precursor with hydrophobic graphene-based structures (Ref [30]) and deposition of low surface energy rare earth oxides (Ref [33, 34]) have shown increased hydrophobicity. The chemical treatment as a decisive step often is employed as post-treatment to avoid technical difficulties or unwanted heat-sensitive components degradation by high heat input in the thermal spray processes (Ref [32]). Here, the potential of cold spraying with a significantly lower process temperature can be a game changer; it is possible to preserve the valuable phases in initial feedstock, heat-sensitive components and desired properties (Ref [35]). Cold spray can also address the in-service operational challenges; in a majority of applications, a coating made of a single material may not meet the requirement of service expectations, while functionality can be adjusted through designing a composite structure (Ref [36-38]). Moreover, cold spraying offers repairing possibility of the damaged part as another potential benefit; cold spraying is a green technology that uses inert gas, electric heating source with limited heat generation, capable of depositing coatings with desired mechanical properties without post-processing (Ref [35, 39-41]). Despite its many benefits, cold spraying is not as much explored as thermal spraying for fabricating non-wetting surfaces. (Ref [18, 25, 42, 43]). These advantages can be used for successful fabrication Al-based alloys (Ref [44]), as widely used engineering alloys used in industry with naturally hydrophilic behavior (Ref [45]).

In the current research, the aim was to incorporate micron-sized quasicrystalline (QC) powders into metallic coatings to alter their wetting performance toward hydrophobicity. Quasicrystalline materials with unique lattice structures have shown interesting physical and chemical properties different from well-known crystalline networks (Ref [46]). Studies on the properties of quasicrystalline materials have revealed sophisticated functional properties such as low surface energy, low friction coefficient, low conductivity, considerable hardness and electrochemical resistance (Ref [47-50]). Evidently, this category can be considered as candidate material for the fabrication of hydrophobic surfaces. Although thermal spray processes like high-velocity oxygen fuel (HVOF) and plasma spraying have been successfully employed in the deposition of hard and brittle quasicrystalline powders, the

phase change during the high-temperature deposition is a constant challenge (Ref 51, 52). Furthermore, using QCs as reinforcing components in composite structures is a preferred strategy for avoiding mechanical problems caused by the inherent brittleness of these particles. A majority of the works reviewed in (Ref 53) have used powder metallurgy followed by sintering of compressed geometry or cooling rate-controlled melt solidification through conventional metal processing technologies for composite structure fabrication. Regarding the demonstrated capability and flexibility of cold spraying in composite production, our literature review revealed a possible knowledge gap due to the small number of studies, most of which largely focused on tribological and mechanical characteristics assessment (Ref 52, 54-56). Exploring the wetting characteristics of cold-sprayed QC-containing coating established the basis of this study, reflecting the practical interest in producing functioning surfaces.

Coatings were produced by using pre-mixed Al-based QC powders and Al6061 (metallic powders) with a high-pressure cold spray system. Surface features, including topography, surface roughness and surface wettability of the coatings, were studied to evaluate surface properties of these Al-QC composites compared to metallic cold-sprayed Al6061 coatings. The potential linkages between the cold spray procedure and the produced microstructural characteristics are then thoroughly addressed. Ultimately, regarding the sustainability and potential of cold spraying in repair of these surfaces, erosion artifact on cold-sprayed coatings, and subsequent coating refurbish was carried out to provide a general picture of the restoration capabilities of the developed coating.

Experimental Procedure

Feedstock materials and coating process

Three different powder compositions were selected with the following specifications: gas atomized aluminum alloy (Al6061, 10–40 μm as particle size distribution of d10-d90) supplied by TLS Technik GmbH & Co. (Bitterfeld, Germany) and two different size range of quasicrystalline Al-based powders (Cristome A1 with a nominal composition of Al53.9- Cr15.5- Fe13.8-Cu17.5 wt%, 10–30 μm called fine QC and 20–70 μm named as coarse QC, hereafter) supplied by Saint-Gobain Coating Solutions (Avignon, France). A high-pressure cold spray system, PCS-100 (Plasma Giken Co., Ltd., Saitama, Japan), mounted on an ABB robot arm (ABB Ltd., Helsinki, Finland), with nitrogen as the propeller gas was employed to accelerate the particles toward an Al-alloy plate vertically fixed as the substrate. For the composite coatings, the desired portion of each feedstock material was taken and mixed in a container and physically blended before transferring to the powder feeder (Plasma Giken Co, Ltd., Saitama, Japan. Table 1 contains the cold spray process parameters and sample coding for the investigated samples that were selected based on the preliminary testing with different compositions and process parameters. The codes in the table being used frequently in the text are generated based on the following argument: AlX-yQC where X is the volume percentage of Al6061 powders in the initial blend and y represents the size of QC powders that can be coarse (c) or fine (f). The substrates were degreased with ethanol and grit blasted using alumina grits (Mesh #40) prior to spraying the samples. An electrical heating plate was positioned behind the substrate allowing the surface temperature of the substrate to be stabilized ($\sim$ 100 °C) before beginning the spray procedure. This heating method was chosen based on previous coating optimization experiments that demonstrated the effects of in situ heat treatment on the microstructure and coating performance. A laser backlight-illuminated monitoring system, HiWatch HR2 (Oseir Oy., Tampere, Finland), was used to gain a better understanding of particle mobility in the gas stream. Feedstock materials were sprayed with the parameters used in coating fabrication without substrate while the stand-off distance (SoD) was set as the span of nozzle exit to focus plane of the laser system. The process started with real-time monitoring until the following criteria were fulfilled;

Table 1 Sample codes, feedstock materials, process parameters and substrates used for cold spray coating production

Code	Feedstock Materials	Process parameters							
		P (bar)	T (°C)	SoD (mm)	Step (mm)	Feed (rpm)	Speed (m/ min)	Layers	Note
Al6061	Al 6061 10–40 μm								
Al25-fQC*	25 vol% Al6061 + QC A1 **10–30** μm								
Al10-cQC**	10 vol% Al6061 + QC A1 **20–70** μm	20	450	40	1.5	3	5	3	
Al50-cQC	50 vol% Al6061 + QC A1 **20–70** μm								
Al50-fQC	50 vol% Al6061 + QC A1 **10–30** μm								Used in repairing trial

* fine quasicrystalline powders ** coarse quasicrystalline powders

mean particle velocity value stabilized and at least 1000 particles were detected by the camera. Then, the recording started by capturing the 50 frames with 400-ns laser interval. More details about the diagnostic of cold spray process are provided in earlier work (Ref 57). The acquired data were processed in Origin 2019b 9.6.5.169 software (OriginLab Corporation, Northampton, MA, USA) by plotting 2D kernel density graphs as a nonparametric technique to estimate density of scattered points.

Characterization

A scanning electron microscope (SEM) (JEOL-IT500, Tokyo, Japan), operating at a 15 kV accelerating voltage, was utilized to observe the microstructure of selected test pieces. Secondary electron (SE) and backscattered electron (BSE, stereographic (BSE-S) mode) detectors were used to characterize the microstructure. The stereographic mode can concurrently accentuate compositional contrast and topographical characteristics, which are highly informative for composite surfaces. A parallel sample of each coating made in the same spray round was cut through the cross section using a precision cutter. Cross-sectional SEM samples were prepared by traditional metallographic methods including grinding and polishing of mounted specimen. ImageJ software package was utilized to measure the thickness and compare porosity level via at least five individual measurements. Surface roughness information was retrieved from an optical 3D profilometer, Alicona InfiniteFocus G5 (Alicona Imaging GmbH, Graz, Austria), with a focus variation working mechanism. The measured datasets from the desired area were scanned using Imagfield measurement by stitching 10×10 single measurements (100 neighboring zones with area = 2.81*2.81 mm^2

with overlapped boundaries). The final datasets subsequently were processed in the IF-MeasureSuite V 5.1 (Alicona Imaging GmbH, Graz, Austria), after form removing through the robust method. Primary datasets were used to visualize the surface texture, and the roughness component was filtered by a selection of proper cutoff wavelengths, following the approach employed in the literature (Ref 58) to extract relevant surface parameters.

Droplet shape analysis (DSA)

Sessile droplet static contact angle (CA) measurement was taken (room temperature 23.5 °C $\pm$ 2 °C, relative humidity of 50 $\pm$ 5%) using a droplet shape analyzer system (DSA100, Krüss, Hamburg, Germany). The procedure for CA measurement consisted of transferring a 5 µl droplet MilliQ ultra-high purity water (Millipore Corporation, Bedford, MA, USA) to the coating surface. Apparent CA was measured from the side view images taken from the shadows of at least 6 individual water droplets in the automatic procedure. Deformation of 10 µl droplets fallen from 10 cm height upon impact to the surfaces was visualized by installation of a 4000-fps high-speed camera (Memrecam fx K5, nac Image Technology, Salem, MA, USA) equipped with a 60-mm Nikon lens alongside a monochromatic light source at the side view of the stage. Before droplet shape analysis, the samples were cleaned with ethanol in an ultrasonic bath for 3 min to eliminate surface contamination and dried by cool air flow to accelerate the evaporation of ethanol. The samples were maintained in a desiccator cabinet for 1 day to assure removal of water content trapped in the coatings and later on, they were kept in the controlled condition room until the test day.
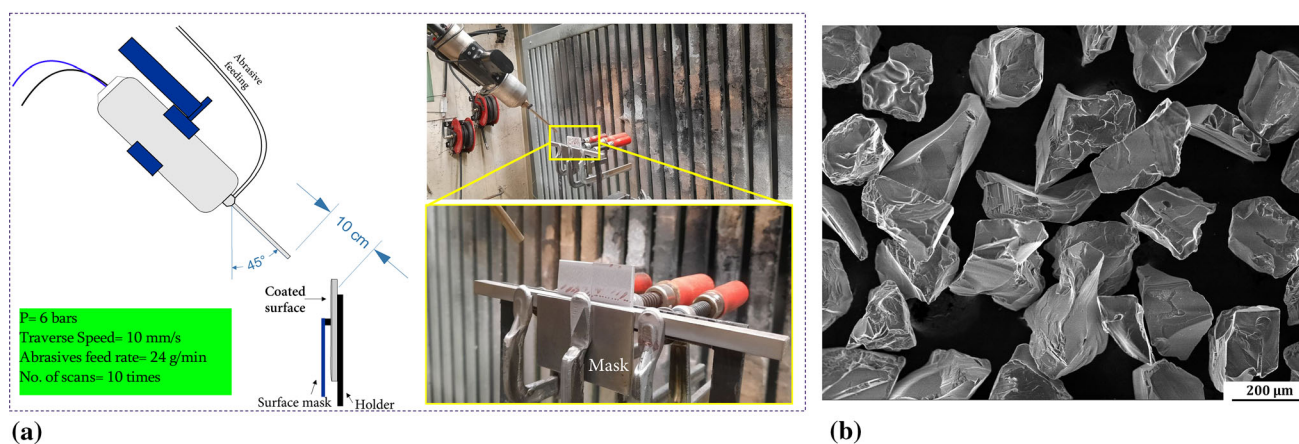

Fig. 1 (a) The setup and process parameters used in defect creation by low-pressure cold spraying of abrasive alumina particles and (b) morphology of alumina particles used as abrasive media

Defect formation and repairing strategy

A simplified plan was contrived to examine the viability of restoring the coating functionality by repairing the damaged part via cold spraying. A composite-coated specimen and a counterpart from aluminum alloy coating (Al50-fQC and Al6061, see Table 1) were fixed on a vertical plate and masked using a metal plate. A Dymet 403 (Obninsk Center for Powder Spraying, Obninsk, Russia) low-pressure cold spray system with air as the working gas and provided process parameters in Fig. 1(a) made an artificial defect on samples by eroding a 1.8 cm wide band. Inclined collision of coarse alumina (Al_2O_3) particles with faceted morphology, sharp corners and angular edges according to features shown in Fig. 1(b) is likely to cause sufficient material removal (Ref 59). Therefore, the impact direction was set as 45° between the abrasive flow direction and coating surfaces. The damaged parts were recoated with two layers of Al50-cQC coating composition without heating the substrate. (The rest of process parameters are described in Table 1.) Wettability assessment and microstructural characterization were conducted on eroded band and repaired parts. In addition to optical surface roughness measurement of the desired area, a complete scan of each sample was measured in each phase and processed using the *DifferenceMeasurement*-module in IF-MeasureSuite software to evaluate the difference induced by each alteration. The datasets were finely overlapped using N point alignment in the intact area that was under mask during erosion and repair. Next, the difference between the datasets was extracted by a 3 μm threshold. The volume changes in the eroding band were then computed. Repaired sections were prepared using standard metallography procedure and observed using SEM and profilometer to probe the soundness of the deposits. Inspired by procedure used in (Ref 60, 61), interfacial Vickers indents with 0.5, 1, 3 and 10 kgf load were landed on the damaged/repaired interface using hardness testers (MMT-X7, Matsuzawa Ltd., Akita, Japan & Duramin-A300, Struers, Copenhagen, Denmark) for qualitative evaluation of interfacial adhesion.

Results

Feedstock Characteristics

Figure 2 represents the morphology of feedstock powders. Quasicrystalline (QC) powders were generally spherical with slight deviation in geometry in two size ranges of coarse (Fig. 2a) and fine (Fig. 2b). The QC powders surfaces possessed analogous surface textures and features. The sporadic presence of satellites, small particles attached to main powders, can be detected in both distributions. Gas atomized Al6061 powder particles were spherical (Fig. 2c), with smoother surface texture and more satellites attached to larger powders compared to QCs. Both QC and Al6061 feedstock powders have random irregular particles marked with arrows in Fig. 2 (a-c).

Figure 3(a) displays the HiWatch HR2 set up used for measuring the velocity of in-flight particles and heat-contour map of the particle velocity versus the position of particles in respect to the nozzle centerline (Fig. 3(b)-(d) for Al6061, coarse QC particles and Al10-cQC feedstock combination, respectively). A symmetrical distribution from the centerline of nozzle (X = 0) indicates that in-flight particles velocity of particles located near the core of jet have greater velocity. The mean velocity of particles was found to be lower than measured in-flight velocity of similar feedstock materials sprayed with higher temperature (Ref 44). It is noteworthy to emphasize that using a same set of cold spray process parameters for Al6061 and composite structure was meant to avoid process parameters influence on coating formation.
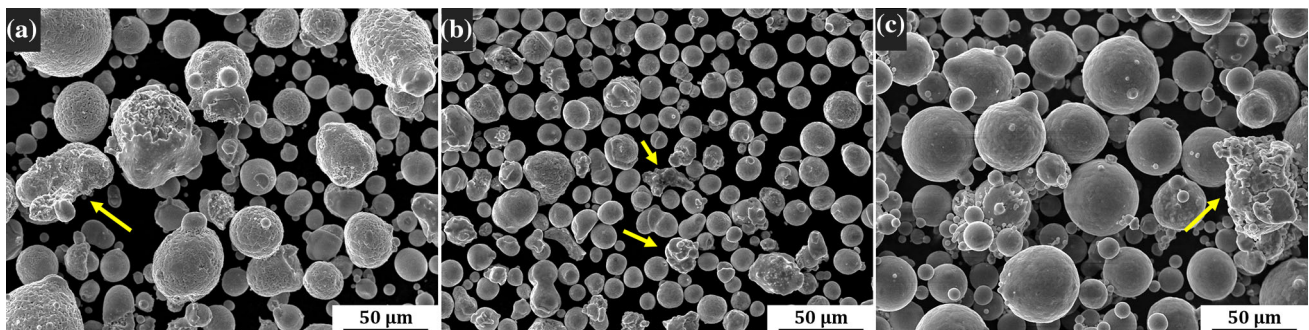

Fig. 2 SEM-SE images of powder morphologies of (a) coarse quasicrystalline, (b) fine quasicrystalline and (c) Al6061 feedstock materials. Irregular particles are marked with arrows
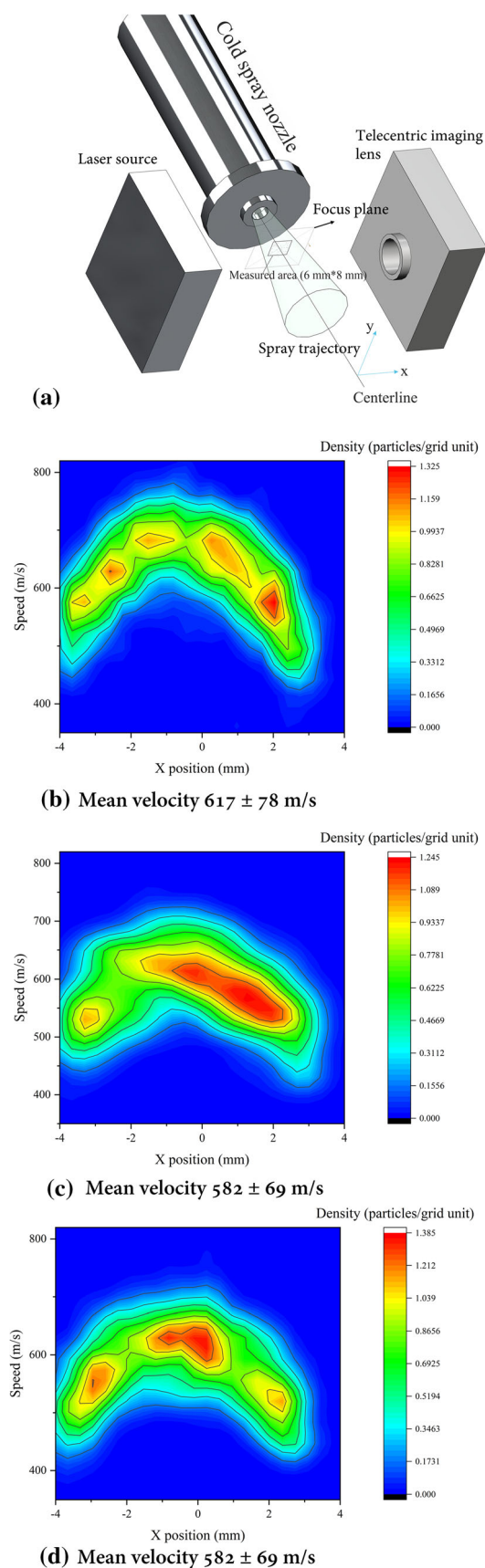
(a)

(b) Mean velocity 617 ± 78 m/s

(c) Mean velocity 582 ± 69 m/s

(d) Mean velocity 582 ± 69 m/s

◄**Fig. 3** In-flight particle velocity versus their position in the gas stream at 40 mm distance from cold spray de Laval nozzle exit with fixed process parameters P = 20 bars, T = 450 °C: (a) Schematic view of velocity measurement setup, (b) Al6061, c) Al10-cQC combination and d) Coarse QC particles. X = 0 corresponds to the centerline of nozzle exit or gas stream

Microstructural properties of coating surface

Figure 4 shows the microstructural features of examined surfaces. Spherical particles are frequent at the surfaces with visible particle boundaries from the last impacted particles. Nevertheless, underneath scattered spherical particles on the surface, denser structures were also generated by particles flattening through high-velocity impact that caused more deformation. In general, a wavy and rough topography was found all over the surface of cold-sprayed Al6061 coating.

The QC-Al composite surface formed where QC particles with heavier mean atomic mass appeared as the bright phases. Low magnification views of composite coatings in Fig. 4 illustrate a random distribution of QC particles over the composite surfaces. The higher magnification of Al10-cQC and Al50-cQC topography in Fig. 4 shows the dominancy of random craters as large as the coarse QC powders that hammered the surface and rebounded with micron-size fragment pieces leftover. Intact and fractured QCs, fragments and rebounded zones concomitantly exist on the examined composite surface. Exceeding fragmentation velocity—the velocity at which transition from rebounding to fragmentation takes place—is recommended to have a high content of brittle phase during cold spraying, although it leads to rarely intact particles left at the surface (Ref 62). The co-deposition strategy using a mixture of powders can help to contain a fraction of QC particles pinned in the structure in its original morphology as well. Material flow at the edges of the craters can be seen regularly all over the surface.

Using finer QC particles in the initial powder feedstock mixture revealed a slightly different morphology on the composite surfaces. Smaller in size but higher in number, rebounded zones in Fig. 4 generated a finer dimple-like features over larger scale dome-like structure. The rough top surface made it difficult, if not impossible, to accurately measure and compare the relative content of each phase. In addition to the roughness that interferes with image processing, the minute, dispersed bits of QC powders clinging to the soft phase are difficult to account for in the image analysis.

Multiscale surface textures, consisting of large-scale waviness and micron-scale roughness, were generated through cold spray process. This is a typical surface
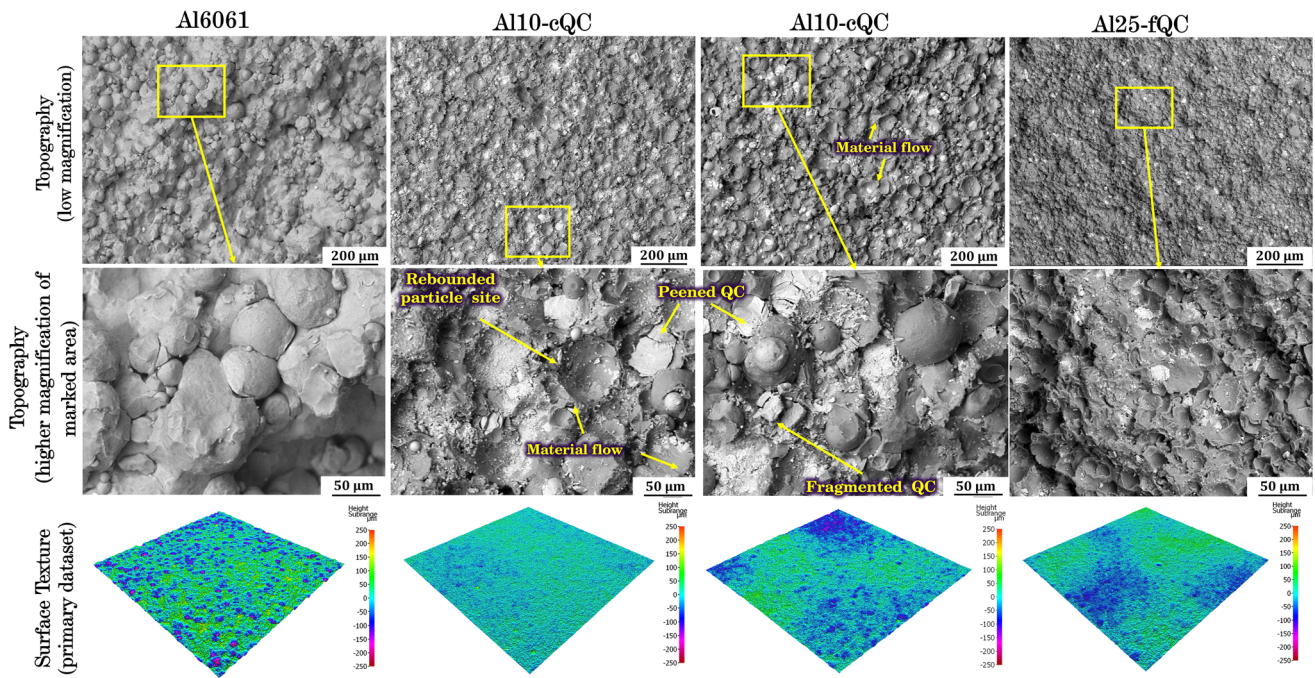
Fig. 4 Morphology (BSE-S micrographs) and primary surface texture of cold-sprayed coatings tested for wetting behavior. The visualized texture is the form-removed primary dataset from examined 2*2 cm^2 area measured by optical profilometer
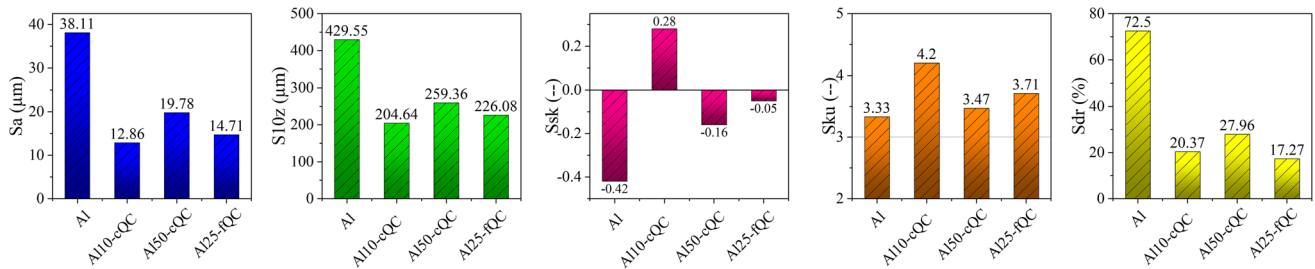

Fig. 5 Areal surface roughness parameters of the sprayed coatings

characteristic of sprayed coatings (Ref 28, 63). The surface features including deformed, semi-deformed, fragmented particles or rebounded zones varied by feedstock materials used. The variation can be tracked in disparity of the surface parameters. It is established that 2D parameters extracted from line scan of the surface, including Ra value which are popular in industry, fail to describe the real surface features (Ref 58, 64). Since the surfaces of cold-sprayed coatings are considerably inhomogeneous, the Ra values showed scatter results depending on the zones that the interest line crosses. On the contrary, surface parameters have proved distinct advantages and surplus opportunities to relate the functionality of surfaces (Ref 64). Therefore, it is reasonable to shift the focus toward surface parameters and comprehend their meaning.

The areal surface roughness parameters for the studied coatings are presented in Fig. 5. Sa, described as the height amplitude of the selected area, is a commonly used surface parameter. Sa generally is an indication of surface roughness and correspond to definition of Ra in the line profile scan. Sp, Sv and their sum Sz are other height parameters representing the maximum peak height, the deepest valley depth and maximum height of the selected surface. S10z is an extended parameter that corrects outlier influence on the measured area by considering five tallest peaks and five deepest valleys in the calculation of the largest heights. Information regarding the distribution of height can be explained by skewness (Ssk) and kurtosis (Sku). In positively skewed (Ssk > 0) surface high peaks dominate at the surface while negative Ssk implies that surface is mostly made of deep valleys. The kurtosis value defines the sharpness of irregularities where surfaces with Sku > 3 and Sku < 3 have sharper and blunter features, respectively, while Sku = 3 means equal distribution of blunt and sharp asperities and valleys. Sdr is defined as the developed interfacial ratio implying the surplus area generated by

surface roughness. Based on these definitions extracted from ISO 25178–2 standard and used in the literature (Ref 58, 64), variation of the selected surface parameter can be linked to microstructural features. Cold-sprayed Al6061 coating shows high Sa and S10z values. But for cold-sprayed composite coating, these values declined with increasing content and size of QC particles used in the feedstock. As explained for the morphology of surfaces (Fig. 4), plenty of undeformed or less deformed particles appeared at the surface of coatings with less tamping or hammering effect, giving rise to Sa and S10Z values. On the other hand, the high-velocity impact of hard QC particles causes severe plastic deformation and material flow on the rough surface of the underlying layer. Therefore, that taller asperities are flattened, and valleys are filled with the flow of deformed materials. Shape of asperities can be differentiated by distribution sensitive Sku and Ssk factors. Negative skewness means that valleys have dominancy over the peaks at surface. Allegedly, the Ssk value reduces with increasing the number of open pores (Ref 65). Accordingly, the skewness of the surface was also influenced by the QC content of feedstock blends. All surfaces indicated the presence of sharp-cut asperities with Sku >

3; Al10-cQC and Al6061 coatings had the highest and lowest Sku values among the tested samples, respectively. Possible factors in ranking the order of kurtosis value of the coating surfaces could be the jets at the crater edge of non-adhering particles, fractured particles sharp edges and sporadic fragments. In brief, Al6061 coating showed remarkably high surface roughness with a large difference between the peaks and valleys, which caused a significant increase of real surface area. Regarding surface roughness parameters, cold-sprayed composite coatings typically had smoother surfaces, smaller but pointier asperities, and less additional surface produced by roughness than the cold-sprayed Al6061 coating had. The dominance of peaks at the surface of Al10-cQC produced by the severe hammering of structure is a notable distinction between surfaces. Surface roughness measurements showed a clear difference between Al10-cQC and Al50-cQC, indicating that an increase in QC content in the feedstock materials led to a decrease in roughness and creation of additional surfaces.
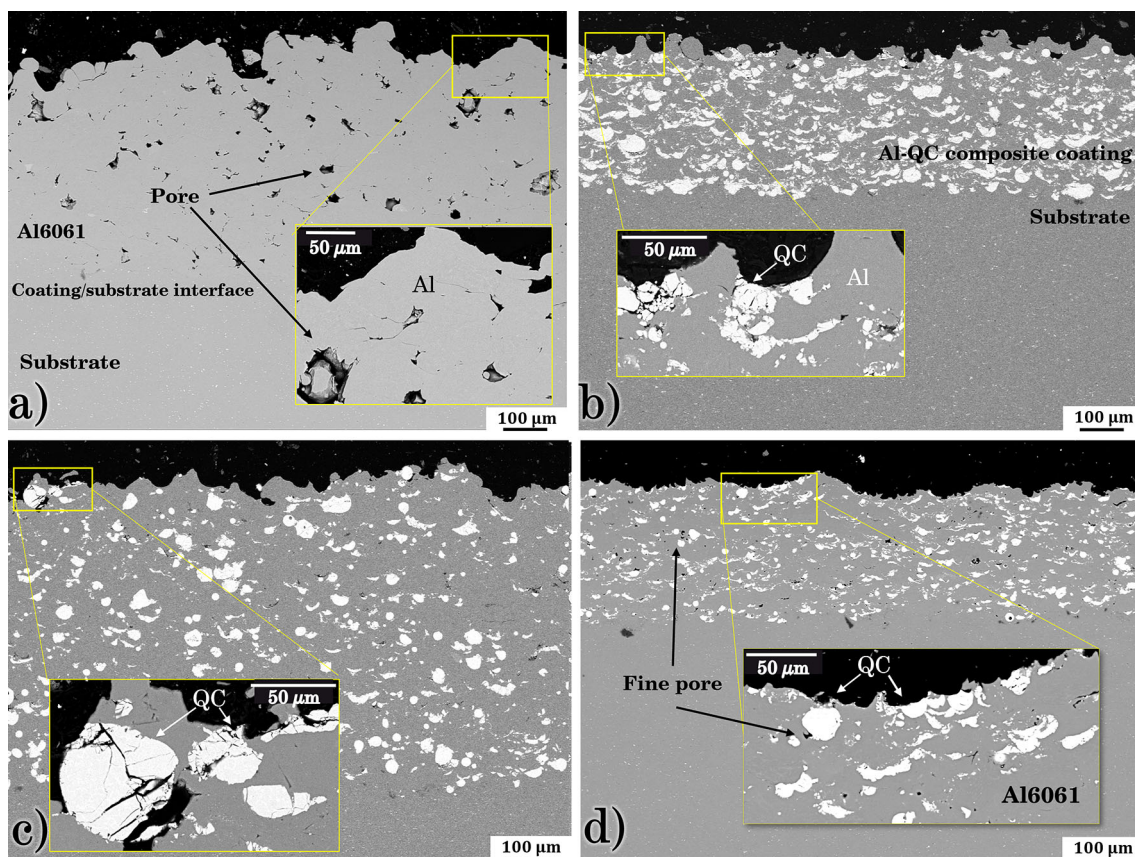

Fig. 6 SEM-BSE images representing cross-sectional features of a) Al6061, b) Al10-cQC, c) Al50-cQC, and d) Al25-fQC. Inset micrographs are higher magnification of the marked areas

Microstructural Characteristics of Coating

Cross section of the cold-sprayed Al6061 sample (Fig. 6a) revealed a thick deposit (514 μm ± 78 μm) due to relatively high deposition efficiency of ductile aluminum particles (Ref 35, 44), but disconnected random pores (black spots in Fig. 6(a) and corresponding inset micrograph) were found across the cross section, especially closer to the surface where the hammering effect from subsequently impacted particles is marginal (Ref 36. The cross sections of composite coatings are presented in Fig. 6(b)-(d). Interestingly, denser coatings with an almost uniform distribution of QC and Al6061 particles were produced. Achieving such an improvement in structure implies the positive effect of QC particles in the densification of the coating, sprayed with the same cold spray process parameters. The volume ratio of QC/Al in the initial feedstock (provided in Table 1) declined within the composite structures due to the rebounding of hard QC powders. Blending of feedstock materials for composite coating formation is a straightforward and feasible method, but the distribution of phases cannot be engineered during the process (Ref 38,66). Comparably, deposition efficiency was lower for the composite coating with higher QC content ($t_{Al10\text{-}cQC}$ = 310 μm ± 16 μm < $t_{Al50\text{-}cQC}$ = 668 μm ± 27 μm). It is noteworthy to mention that the deposition efficiency is estimated by comparing the thicknesses. The notable difference is that, when sprayed with the same cold spray process settings, Al50-cQC exhibits higher coating thickness and densification degree than Al6061 (Fig. 6a and c). Having reinforcing phases in the initial blend of feedstock positively influences the tamping effect and deposition efficiency at the same time (Ref 36). Nevertheless, loading extensive hard particles increases the tamping and densification at the expense of non-effective collision and can decrease deposit efficiency, as deposition is still governed by the ductile metallic phase. The latter was valid for Al10-cQC sample, even though the chosen ratio was intended to maximize QC particle coverage on the top surface. On the other hand, the composite coating containing fine QCs (Al25-fQC) did not show significant improvement in terms of densification and deposition efficiency of the coating compared to counterparts containing coarse QCs (see Fig. 6d). Image analysis estimated the share of QC phase in the cross section of Al25-fQC composite structure at 18.2 vol-%, whereas Al10-cQC and Al50-cQC have higher average values of 50.1% and 19.4%. Coarse QC particles had a higher contribution to the final structure by taking the QC volume fraction of the initial feedstocks into account. The highest QC fraction that was calculated for Al10-cQC was higher than in the earlier researches of cold-sprayed QC-containing composite coatings (Ref 54, 55). Increased porosity has been reported after increasing hard QC content up to 30% in the coating structure (Ref 54). Remarkably, the porosity level was lowest for the coating with the highest QC content; all coatings were denser than the Al6061 coating with 2.82 ± 0.74 vol% porosity, although QC particle size had a greater influence on void reduction (average pore vol% excluding the outliers near interfaces of cross sections: Al10-cQC < 0.10 pore vol%, Al50-cQC = 0.24 ± 0.09 pore vol%, Al25-fQC = 0.95 ± 0.27 pore vol%). These findings support the argument that larger particles with more inertia have better tamping or hammering effect of the coatings upon impact (Ref 67).

Wetting Assessment

Figure 7 depicts selected droplet shadow side view frames that were utilized to determine the droplet CA. Cold-
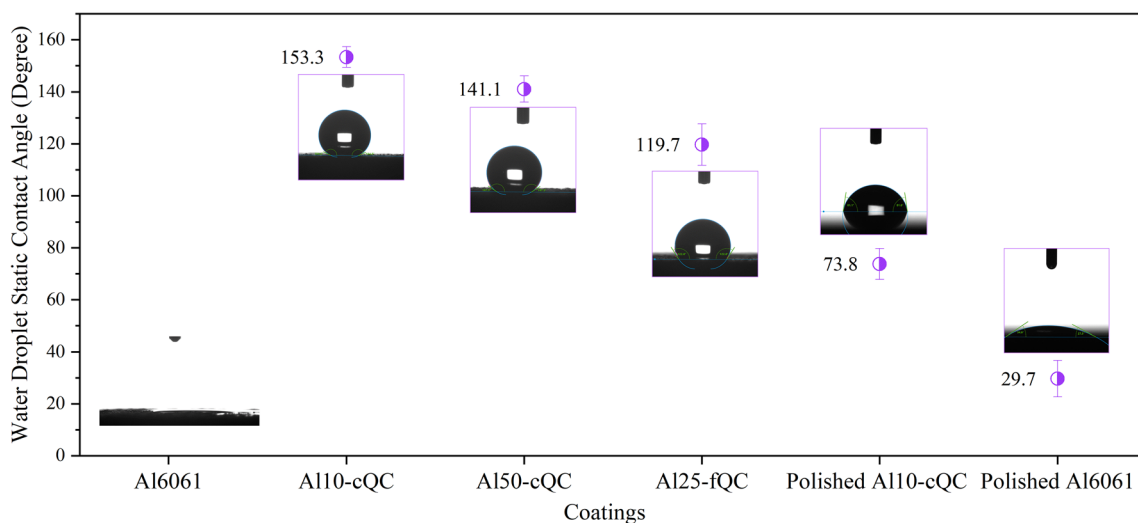

Fig. 7 Droplet shape and static CA of water droplet on tested surfaces

sprayed Al6061 coatings showed hydrophilic behavior; water droplets tended to continuously spread shortly after placing on the surface. Visually, wetting marks multiple times larger than original droplet diameter appeared after the disappearance of the water droplet on surface. A possible reason could be the microstructure of coating with connected network of pores and heterogeneities that helps spreading water through narrow pathways (Ref 68). Furthermore, the hydrophilic nature of untreated aluminum alloys has been already confirmed (Ref 23,69). It has been also found that keeping the bulk aluminum alloy in atmospheric conditions slightly increases the CA due to absorbance of airborne organic compound from the atmosphere. However, in all trials of water on cold-sprayed Al6061, surface showed the vanishing behavior with CA < 10° after sample storage in the atmosphere more than 6 months.

On the other hand, composite coatings showed drastic increase of CA and all values were higher than 90° which is an arbitrary, but commonly accepted, threshold for hydrophobicity. Al10-cQC had the highest CA exceeding 150° followed by Al50-cQC and Al25-fQC with CA ∼

141° and 120°, respectively. The standard deviation for multiple CA measurements (the error bars in Fig. 7) was low for each surface implying a homogenous wetting all over the surfaces. The CA values remained constant up to 30 min after droplet positioning. Despite high CA, droplet mobility was not observed for composite structures in roll-off or sliding CA conditions. The droplet remained pinned to surfaces even after tilting of the stage exceeding 30°. Similarly, despite an increased CA, limited droplet movement is reported in several research works (Ref 33, 42, 69).

In the previous section, it was mentioned that surface roughness and chemistry (QC/Al at surface) are tightly interconnected to the feedstock combination used. To confirm the role of roughness/texture on hydrophobicity, Al6061 and Al10-cQC wetting behavior was compared after analogous mechanical polishing of their counterpart surfaces. In polished state, the Al6061 and composite coating showed hydrophilic state. Al10-cQC lost its hydrophobicity (CA = 64.8 ± 6°) after removing the roughness of surface, and Al6061 gained relatively stable CA up to 30° (see Fig. 7). Evidently, surface roughness effect is significant though the quantitative
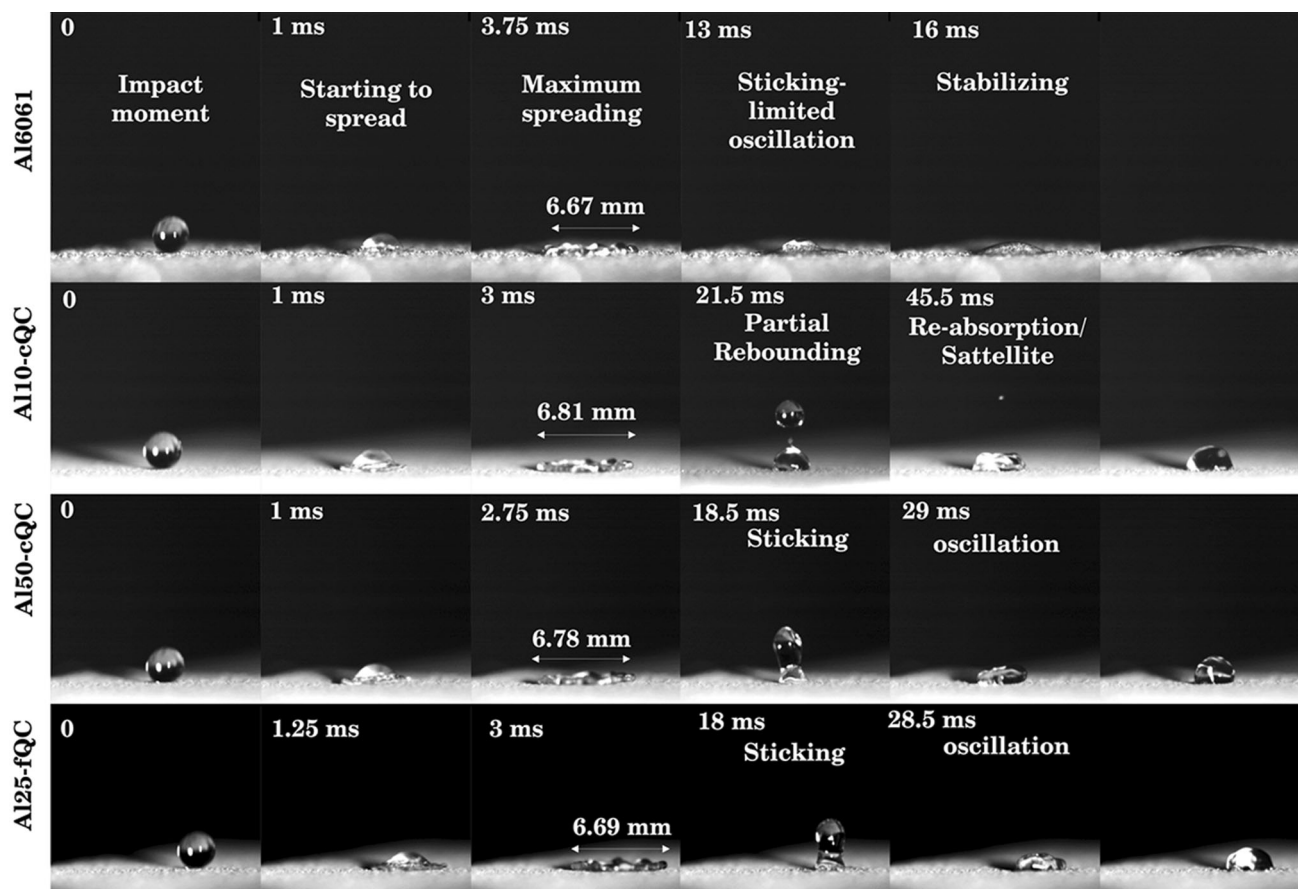

Fig. 8 Sequential images of water droplet (d = ∼2.4 mm) impact (V = ∼1.1 m/s released from 10 cm height) and its dynamic behavior on the tested surfaces. Impact instant set as zero and respected frame timing are adjusted accordingly. Slow motion video regarding to impacts are provided as supplementary materials

surface roughness parameters (Fig. 5) did not show a direct correlation or trend in composite surfaces.

Interaction of surfaces with the impacted water droplets provides additional information regarding the wettability of tested surfaces. Deformation of water droplets upon impact on horizontally fixed coating surfaces has been visualized with high-speed optical imaging. (Videos captured from impacted droplet are provided in supplementary materials.) Selected frames in Fig. 8 contain information about the deformation state of the droplet at a recorded time, measured from first contact between the droplet and surface. From the contact point, droplets began to flatten radially over all surfaces, and the contact area for each case increased until the maximum spreading state was reached. Starting the recoiling phase, the difference between surfaces emerges through dissimilar recoalescence of spread droplets. On composite coating surfaces, the radial momentum changes direction to an upward direction and forces the droplet to detach from the surface. Tendency to rebounding was observed, although partial rebounding happened only on Al10-cQC, confirming higher repellency among the tested surfaces. The droplet was divided into two large segments and several smaller satellite droplets. The detached component rejoined the pinned portion, and oscillation proceeded without further bouncing. The impacted droplets on the other composite coatings failed to rebound and adhered to the surface. On the other hand, Al6061 coating surface prevented water droplet recoiling and preserved the spreading dimension near the maximum spreading diameter. During water spreading and recoiling, the kinetic energy of the droplet dissipates to compensate for the interfacial forces (droplet-surface interactions), which are higher for hydrophobic surfaces. Consequently, the kinetic energy is insufficient to reassemble the droplet and cause it to rebound off the surface (Ref 68). The droplet settled in the flattened form at the surface while the droplets stayed pinned on composite surfaces with hemispherical contour and prolonged oscillation till the end of recorded frames. Noteworthy to mention that the final droplet image in Fig. 8 for each trial was the end frame of the trigger. Visually, their final state possessed reduced CA with a larger area wetted underneath of droplets compared to their CAs in Fig. 7 where the droplet was gently placed on the surfaces. One possible reason according to experiments carried out on pillar textured surfaces (Ref 68) could be the influence by impact kinetic energy, which increased water droplet penetration into surface features in the impact zone, causing sticking and wetting of a broader area.

Repairing the Artificial Defect

The idea of repairing the damaged part was initiated via mimicking a significant surface damage through creating erosion artifacts. The surface of Al6061- and Al50-fQC-coated samples was characterized after a certain area of each piece was eroded by sharp alumina (Fig. 9). The texture presented in Fig. 9 results as a calculation of the difference between datasets before and after erosion. The intact parts of the tested specimen in greenish texture are set as zero level, and deviation from the initial state is highlighted by a depth color map; for example, deep grooves (depth higher than 100 μm) are pronounced in eroded bands of both coatings and are highlighted in blue spectrum color. Morphology of the sample has changed significantly by erosion marks appearing in SEM images; abrasive scars, including ductile scoring, material smearing (marked by arrows) and intruded abrasive alumina particles, were found. QC particles in the composite coating were not detached from the composite structure, and the abrasive path continued over QCs rather than detaching particles, as it is presented in Fig. 9(b) III. Visually, the number of intruded abrasives in the composite coating was found to be lower compared to Al6061 eroded band during the scan of the whole surface using SEM. The volume loss measured in the eroded region was another distinction worth noticing. The volume removed from the Al6061 coating was 41% higher than from the composite coating. It is worth recalling that the composite coating had the least QC particles inside the structure among the studied samples in this work. Due to currently limited information, a direct conclusion about enhanced abrasion resistance of composite coatings is not possible.

Water droplets had the same behavior on both eroded surfaces, although QC particles retained at the structure has an influence on chemical composition. Assuming the fact that erosion occurred at low temperature had a negligible influence on the chemical characteristics of the surface, the intruded alumina abrasives that intermittently emerged at the surface might be a tangible factor affecting the surface chemistry. In contrast, the surface parameters of the eroded regions are comparable independent of their as-sprayed surface parameters (see Fig. 5) and compositions (Al6061 eroded band: $Sa = 12.5$ μm, $S10Z = 155.5$ μm, $Ssk = 0.0$, $Sku = 3.2$ and $Sdr = 47.3\%$; Al50-fQC eroded band: $Sa = 10.4$ μm, $S10Z = 131.0$ μm, $Ssk = 0.02$, $Sku = 3.34$ and $Sdr = 43.3\%$). This discovery once again underscored the significance of surface features in conjunction with the presence of QC particles as determinants in shaping the droplet and its CA.

Figure 10 illustrates the structure and shape of the water droplets on the surfaces repaired by cold spraying of Al50-cQC. The 3D texture profile provided in Fig. 10 I represents the difference of repaired and eroded samples. Successful and consistent coating build-up entirely covering the eroded strips can be confirmed using the color gradient and by setting purple color as zero level corresponding to
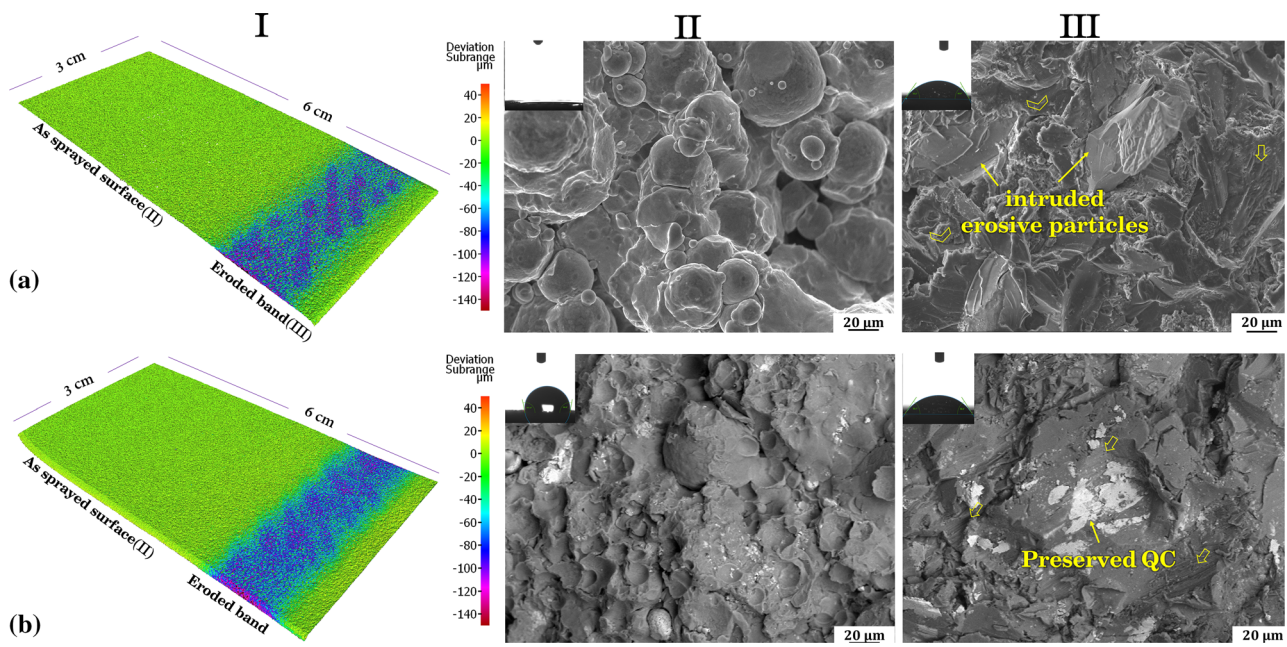
Fig. 9 Alteration of surface of a) Al6061 and b) Al50-fQC coating by abrasive erosion. I) The texture difference between eroded state and as received state, II) Surface morphology in as received state and III) Surface morphology of eroded surface. Chevron marks indicate material smearing and arrows highlight the ductile scoring. Water droplet shape is provided on corresponding image
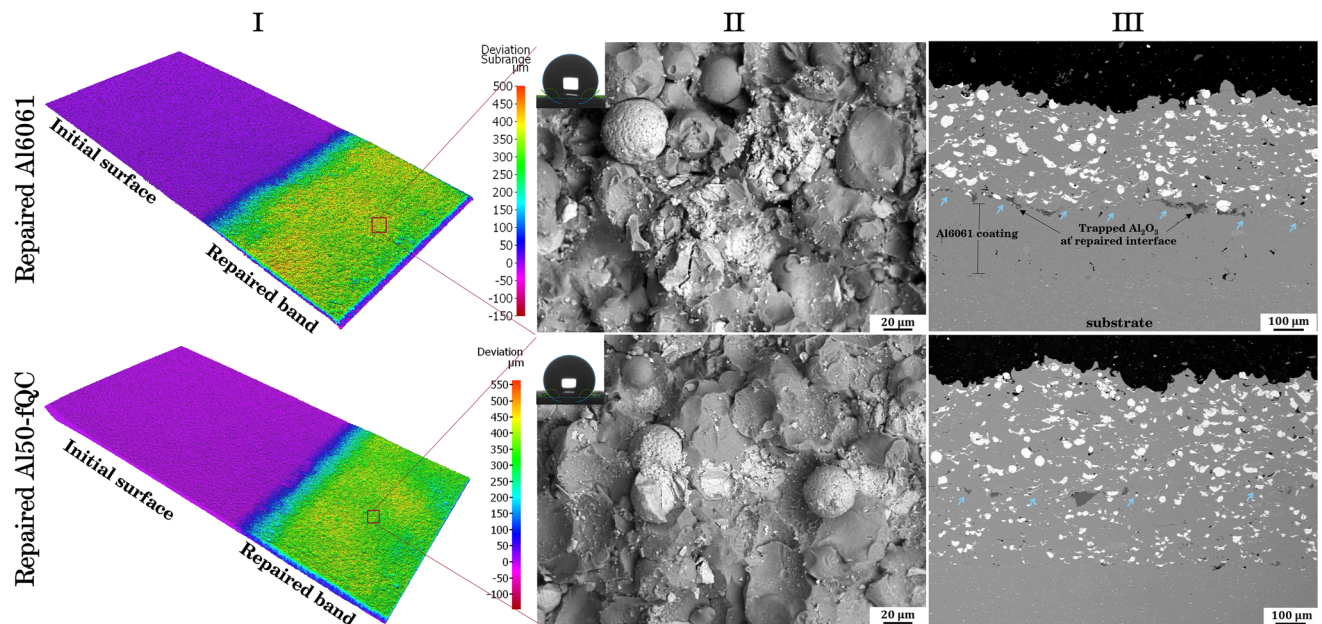

Fig. 10 Repaired coatings. I) The texture difference between repaired and eroded state, II) Surface morphology of repaired coatings and III) Cross section of repaired coatings. Water droplet shape is provided on corresponding image

the masked intact area. Visually, restored surfaces exhibit waviness resembled to that of sprayed coatings on grit-blasted substrates, with no discernible effect from the eroded layer roughness/waviness. Furthermore, topographical characteristics on the surface of mended portions were almost identical. Deformed Al6061 powders, rebounded impact zones, non-deformed QC particles with their original texture, fractured and fragmented QC particles altogether can be found on the surface (Fig. 10II). These findings validate the similarity between the water droplet forms and intimate CAs observed on both surfaces. Both repaired coatings revealed the average water droplet CA comparable to Al50-cQC coatings applied as the
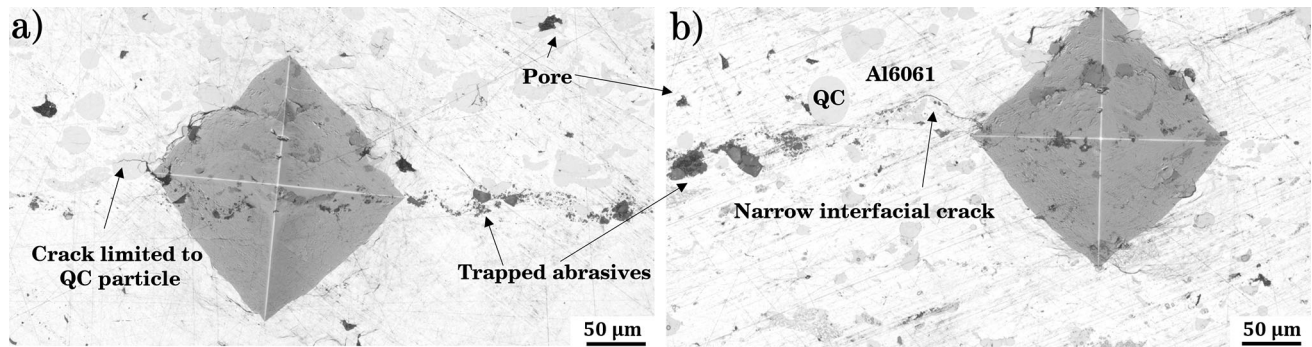
Fig. 11 Interfacial Vickers indents landed on eroded/repaired interface captured by optical profilometer a) Repaired Al6061 and b) Repaired Al50-fQC coatings

coating on plates (CA $_{Al50\text{-}fQC}$ = 141.1°, CA $_{repaired\ Al6061}$ = 134.5°, CA $_{repaired\ Al50\text{-}fQC}$ = 136.2°).

Cross section of the repaired parts in Fig. 10 III indicates that the cold spray process developed a proper bonding between the restored coating and eroded surface for both samples. Trapped abrasives appeared in gray color at the interface of eroded coating leftovers and new coatings. Generally, the bonding of repaired coating to the eroded surface was strong so that interface could only be tracked with the help of the entrapped abrasives. However, no significant effect was observed due to abrasive entrapment in terms of bonding of the repaired coating. Entrapped abrasives do not necessarily interfere with the operation of the thermal sprayed coatings, if not enhance the continuing-substrate adhesion. Generally, grit blasting prior to coating deposition enhances interlocking at the interface of coating with sublayer without meddling with coating properties and surface functionality (Ref 60, 70). At the interfaces, there are no evident signs of delamination or substantial interfacial voids, despite slightly larger pores appeared in the repaired coating compared to their Al50-cQC counterpart sprayed on aluminum plate. Possible explanations include differences in process parameter settings, such as the heating plate behind the specimen, and fewer layer applied in repairing trial (2 layers) compared to Al50-cQC (3 layers) that may result in extra deformation to the underneath structure.

The interfacial indents were used to assess the integrity of repaired interfaces. The indents with loads equal to 1 kgf and less did not propagate visually significant cracks along the interface. Indents landed on random interfacial spots implying a proper interfacial bonding across the studied coating cross section. When loaded by Vickers indents with varying loads, QC particles act brittle and tend to propagate cracks as large as the particle diameter. Nonetheless, the cracks did not extend beyond the indent-landed QC particle (see Fig. 11a with indentation load of 3 kgf). Figure 11b demonstrates a narrow crack follows the interface path once interfacial indent with 3 kgf load was applied. In this

context, material flow and plastic deformation at the edges of indents without tearing the boundaries of adjacent bonded particles indicates a satisfactory level of integrity. Note that higher indentation load (10 kgf) failed to provide a reliable result as it led to enlarged indent marks that exceeded coating thickness. These observations indicate that the repaired parts are well-bonded to the eroded parts.

Discussion

Cold-Sprayed Al-QC Composite Coatings-Microstructure and Wetting Behavior

Investigation of surface wetting is typically accompanied by exploring surface chemistry and roughness. There is a number of studies on surface roughness modification, provided the surface chemistry remains constant (Ref 27, 58). Aside from the fact that even minor surface interaction with the environment might produce chemical changes, establishing a window of surface roughness parameters within which a specific wetting behavior can be seen is not a feasible approach. On the one hand, exceptional hydrophobicity of a suspension plasma-sprayed TiO_2 coating (Ref 27) and, on the other hand, enhanced hydrophilicity of modified TiO_2 surfaces produced by HVOF have been correlated with surface dual roughness (Ref 31). In the majority of cases, the highly hydrophobic behavior of thermally sprayed coatings only has appeared after a further chemical modification of feedstock or coating with hydrophobic agents (Ref 26-28, 31, 42). Thus, the idea of having a hydrophobic surface that requires minimal post-processing was the incentive behind testing different sets of coatings in this work, aiming to engineer a facile production of hydrophobic surfaces by cold spraying.

The cold-sprayed Al6061 coatings produced with the same parameter used for cold-sprayed Al-QC composite coatings demonstrated the highest level of porosity among the tested samples. Al6061 coating has been deposited

efficiently in a range of cold spray parameters that provides a velocity higher than the critical velocity needed for deposition (Ref 44, 67, 71), typically with gas pressure higher than N$_2$ pressure used in this work. Plastic deformation of Al6061 particles took place easier than QC particles; consequently, it acted a binder phase embracing the hard QC particles that are prone to cracking and fragmentation. Similar deformation mechanisms are well-known in cold spraying of metal matrix composites in which the reinforcing component is comprised of hard particles, particularly ceramics (Ref 37). It is found that the removal of weakly adhered particles by the subsequently impacting particles develops jagging features on the surface as the result of remaining fragments (Ref 72). This phenomenon is generally associated with sharp asperities at the surface, as it was confirmed by the results included in Figs. 4 and 5. Compared to Al6061 deposition, the amount of loosely attached and undeformed spherical particles on the surface of composite coatings was lower. Hammering or tamping of previous layers might be considered a favorable influence on densification at microscale, forming the jaggy and dimple-like structure and activating the surface (Ref 37, 74). In Al-QC composite coatings, entrapment of the QC fragments in the structure of the coatings between the passes of deposition, as it was found in Fig. 6 (small bright phases randomly distributed in the coating), might impose effect on the coating mechanical properties (Ref 72, 73). Better understanding of this effect needs further in-depth study on microstructural dependency of mechanical properties.

A steady decline in the CA over time might occur due to the water penetration inside pores and grooves between semi-deformed particles, as has been observed in HVOF cermet coatings with a porous structure (Ref 28). The surface free energy of the material also influences the tendency of water droplets to spread over high energy surfaces or to keep its binding with water molecules and retain spherical droplets in contact with low energy surfaces (Ref 15, 30, 33). Compared to earlier studies (Ref 23, 24), the gradual disappearance of water droplets over cold-sprayed Al6061 coatings in the current study was not surprising.

The concept of wetting has been under investigation for many years, yet there is no general agreement about the underlying mechanisms (Ref 2, 16, 17); Very fine-scale complexity and heterogeneity of real surfaces, nature of liquids and testing condition were found to be sources of deviations from well-known wetting models. Nevertheless, the classic models are still being used to justify the wetting states. Two well-known classical models were proposed by Wenzel (Ref 75) and Cassie-Baxter (Ref 76), which include the roughness of the surface as a critical factor in their explanation. Wenzel has supposed that the infiltration

of water into surface roughness and filling the grooves wet actual area larger than the projected area and causes higher surface energy reduction. Cassie and Baxter have suggested that water cannot fill the whole area under water droplets resting on rough surfaces due to trapped air inside the gaps of rough surfaces. Thus, the droplets stand suspended on top of rough surfaces with air pockets trapped underneath, showing an increased apparent CA and mobility. These models are still being widely used in describing the hydrophobicity evaluations (Ref 15, 21, 27), although there are opposing experimental proofs debating the basics (Ref 77). Here, the *likely scenario* behind the remarkable CA increase can be described as the effect of two factors; crater-like attributes and an overall surface energy reduction generated in the cold spray process:

A) Role of surface roughness: A simultaneous effects of air cushion between gaps in the surface roughness (Cassie–Baxter state, with high CA and high droplet mobility (Ref 9)) and partial penetration of droplets into surface asperities (Wenzel state, with high CA and low droplet mobility (Ref 9)) represent a mixed model. The crater walls and asperities at the surface contributed to the suspension of water droplets over the surface, leading to a high apparent water droplet CA which is in accordance with the Cassie–Baxter state. However, water droplet pinning with high CA is a feature of the Wenzel state. On the other hand, in the Wenzel state condition, roughness should intensify the wetting state, meaning that a hydrophilic material will be more hydrophilic by increasing the surface roughness. However, the pure Wenzel state fails to explain why Al10-cQC composite surface was hydrophobic in the as-sprayed state, and it turned hydrophilic in polished condition. At the same time, droplets pinning follows the Wenzel state. The mobility restriction of the droplet was in line with (Ref 8, 69), which empirically found that having sharp features can enlarge the CA water, while droplet mobility can be compromised. Therefore, a mixed model with partial penetration through asperities might better explain the observation.

B) The presence of low surface energy substances on composites surfaces modifies the total surface energy, giving rise to water droplet CA (Ref 78). QC particles exert chemical heterogeneity to the composite surface, by which the interaction of water molecules with the solid surfaces will be locally different. Whether caused by dissimilar electronic nature of heterogeneities, native oxide films properties or absorption of organic compounds from the atmosphere to the surface (Ref 15, 50), the tendency of the surface to interact with water molecules could

be different. Both the polished surfaces of Al6061 and Al10-cQC were hydrophilic; however, their CA s differed by about 35°. Since the surface alteration was the same, the significance of chemistry could be emphasized accordingly.

Here, feedstock combination caused diverse roughness features and chemical composition at the surface that led to different wetting conditions. Wettability of cold-sprayed Al-QC composite coatings is obvious examples that confirm that the effect of surface roughness and chemistry is synergistic, and it is rather difficult to discuss their individual effects separately.

Feasibility of Repair and Restoring Properties

Coating mechanical properties, facile methods for mass production, applicability for different purposes and long-term stability are some of the challenges in the industry (Ref 1, 19, 20); given that high endurance from cold-sprayed Al-QC could be retrieved, it is also interesting to tackle the other challenges such as extending the functionality. In accordance with earlier studies in cold spray composite structures (Ref 36, 66, 74), QC particles improved the bonding strength and coating density and with specific combinations, it improved the deposition efficiency. However, preserving the properties and refurbishing the components coatings feasibly are also pushing forward to explore them into the structural details.

A number of research works focused on the repairing approach using cold spraying techniques primarily seeking to achieve acceptable mechanical qualities in the restored component (Ref 39, 79). Although it is vital to match the mechanical properties of the main part, repairing should strive to recover other functionalities as well. Regeneration of the structure needs a certain procedure that might be overreaching for delicately patterned or nano-structured coatings (Ref 80). The current results showed that after erosion, hydrophobicity declined due to substantial changes in surface roughness, although in terms of chemistry, QC particles remained at the surface (see Fig. 9b). In turn, repairing the coating was a feasible and straightforward process, which was fruitful in terms of repaired part integrity, substrate type and state flexibility (grit-blasted plate, eroded Al6061 coating, eroded Al-QC composite coating) and hydrophobicity restoration through fast regeneration of the coating layer covering the damaged area without further pre/post-processing. Although the amount of pores appearing in the repaired parts was slightly higher than in the Al-50cQC cold-sprayed coating, by selecting higher process parameters close to what has been used in the earlier works this deviation might be eliminated (Ref 35, 67). Less volume loss is a clue of enhanced erosion resistance of the subjected composite coating, considering some debates on the cold-sprayed composite structure cases (Ref 37, 81) suffering from the reinforcing phase fracture, detachment due to poor interfacial bonding, and debonding of layers under load. Hence, studying tribological qualities is a compelling topic to be continued in the future.

Cold-sprayed Al-QC composite coatings are intriguing because they exhibit enhanced, new or mixed features in comparison with the properties of their constituents. Other combinations may also exhibit improved hydrophobicity; a transition toward hydrophobic behavior was seen for a relatively hydrophilic stainless steel surface—one of the most frequently used materials in structures (Ref 82). It is established that cold-sprayed composite surfaces with QC particles and altered wetting behavior can be expanded to various alloys as well (Ref 82). Nonetheless, a more systematic study is still needed to have a better understanding of coating integrity, structural details and mechanical properties of the developed Al-QC composite structures.

Conclusion

High-pressure cold spraying was used to fabricate composite coatings by feeding different blends of Al-based quasicrystalline and Al6061 feedstock powder materials. The presence of QC particles, in different sizes and content in the cold-sprayed metallic composite coatings surfaces, was found to be a practical approach to change the surface wettability through a one-step process. The cold-sprayed Al6061-coating demonstrated highly hydrophilic behavior in the as-sprayed condition. In contrast, hydrophobic behavior was achieved through incorporation of QC particles in the structure ($119° < CA < 153°$ and tendency to rebound the impacted droplet) owed to the dispersion of low surface energy QC phase on the surface and modification of surface roughness and texture in the cold spray process. The composite coating with a high load of larger QC particles (Al 10 vol-% + QC 20–73 μm) was superior in terms of densification and enhanced hydrophobicity by providing a dimple-like structure with sharp asperities and less open porosities in the structure. Furthermore, cold spraying enabled repairing the artificial erosion damage by successful deposition of well-bonded composite coating without prior surface preparation. The erosion condition using abrasive alumina was chosen as severe enough to cause significant damage and alteration of surface features. The cold-sprayed composite coating structure showed less volume loss due to erosion compared to the Al6061 counterpart. Nevertheless, repairing by cold spray was successful in refurbishing the coating and regaining hydrophobicity.

References

1. A.T. Abdulhussein, G.K. Kannarpady, A.B. Wright, A. Ghosh and A.S. Biris, Current Trend in Fabrication of Complex Morphologically Tunable Superhydrophobic Nano Scale Surfaces, *Appl. Surf. Sci.*, 2016, **384**, p 311-332.

2. H. Yildirim Erbil, Dependency of Contact Angles on Three-Phase Contact Line: A Review, *Colloid. Interface.*, 2021, **5**(1), p 8.

3. T. Young III., An Essay on the Cohesion of Fluids, *Philos. Trans. R. Soc. London*, 1805, **95**, p 65-87. https://doi.org/10.1098/rstl.1805.0005

4. T. Huhtamäki, X. Tian, J.T. Korhonen and R.H.A. Ras, Surface-Wetting Characterization Using Contact-Angle Measurements, *Nat. Protoc.*, 2018, **13**(7), p 1521-1538. https://doi.org/10.1038/s41596-018-0003-z

5. X. Han, J. Li, X. Tang, W. Li, H. Zhao, L. Yang and L. Wang, Droplet Bouncing: Fundamentals, Regulations, and Applications, *Small*, 2022, **18**(22), p 1-19.

6. Y.C. Jung and B. Bhushan, Dynamic Effects of Bouncing Water Droplets on Superhydrophobic Surfaces, *Langmuir*, 2008, **24**(12), p 6262-6269.

7. F. Yeganehdoust, A. Amer, N. Sharifi, I. Karimfazli and A. Dolatabadi, Droplet Mobility on Slippery Lubricant Impregnated and Superhydrophobic Surfaces under the Effect of Air Shear Flow, *Langmuir*, 2021, **37**(20), p 6278-6291.

8. C.R. Crick and I.P. Parkin, Water Droplet Bouncing-a Definition for Superhydrophobic Surfaces, *Chem. Commun.*, 2011, **47**(44), p 12059-12061.

9. Y. Zhu, F. Yang and Z. Guo, Bioinspired Surfaces with Special Micro-Structures and Wettability for Drag Reduction: Which Surface Design Will Be a Better Choice?, *Nanoscale R. Soc. Chem.*, 2021, **13**(6), p 3463-3482.

10. A. Woźniak, M. Staszuk, Ł Reimann, O. Bialas, Z. Brytan, S. Voinarovych, O. Kyslytsia, S. Kaliuzhnyi, M. Basiaga and M. Admiak, The Influence of Plasma-Sprayed Coatings on Surface Properties and Corrosion Resistance of 316L Stainless Steel for Possible Implant Application, *Arch. Civ. Mech. Eng.*, 2021, **21**(4), p 148. https://doi.org/10.1007/s43452-021-00297-1

11. E. Vazirinasab, R. Jafari and G. Momen, Application of Superhydrophobic Coatings as a Corrosion Barrier: A Review, *Surf. Coating. Technol.*, 2018, **341**, p 40-56. https://doi.org/10.1016/j.surfcoat.2017.11.053

12. H. Koivuluoto, C. Stenroos, M. Kylmälahti, M. Apostol, J. Kiilakoski and P. Vuoristo, Anti-Icing Behavior of Thermally Sprayed Polymer Coatings, *J. Therm. Spray Technol.*, 2017, **26**(1-2), p 150-160.

13. R. Mukherjee, A.S. Berrier, K.R. Murphy, J.R. Vieitez and J.B. Boreyko, How Surface Orientation Affects Jumping-Droplet Condensation, *Joule*, 2019, **3**(5), p 1360-1376. https://doi.org/10.1016/j.joule.2019.03.004

14. G. Zhu, Y. Su, P. Bai, J. Chen, Q. Jing, W. Yang and Z.L. Wang, Harvesting Water Wave Energy by Asymmetric Screening of Electrostatic Charges on a Nanostructured Hydrophobic Thin-Film Surface, *ACS Nano*, 2014, **8**(6), p 6031-6037.

15. A. Samanta, Q. Wang, S.K. Shaw and H. Ding, Roles of Chemistry Modification for Laser Textured Metal Alloys to Achieve Extreme Surface Wetting Behaviors, *Mater. Des.*, 2020, **192**, p 108744. https://doi.org/10.1016/j.matdes.2020.108744

16. A.O. Ijaola, E.A. Bamidele, C.J. Akisin, I.T. Bello, A.T. Oyatobo, A. Abdulkareem, P.K. Farayibi and E. Asmatulu, Wettability Transition for Laser Textured Surfaces: A Comprehensive Review, *Surf. Interface.*, 2020 https://doi.org/10.1016/j.surfin.2020.100802

17. Z. Liu, T. Niu, Y. Lei and Y. Luo, Metal Surface Wettability Modification by Nanosecond Laser Surface Texturing: A Review, *Biosurf. Biotribol.*, 2021, **2022**, p 95-120.

18. D. Tejero-Martin, M. Rezvani Rad, A. McDonald and T. Hussain, Beyond Traditional Coatings: A Review on Thermal-Sprayed Functional and Smart Coatings, *J. Therm. Spray Technol.*, 2019 https://doi.org/10.1007/s11666-019-00857-1

19. D. Wang, Q. Sun, M.J. Hokkanen, C. Zhang, F.Y. Lin, Q. Liu, S.P. Zhu, T. Zhou, Q. Chang, B. He, Q. Zhou, L. Chen, Z. Wang, R.H.A. Ras and X. Deng, Design of Robust Superhydrophobic Surfaces, *Nature*, 2020, **582**(7810), p 55-59.

20. T. Verho, C. Bower, P. Andrew, S. Franssila, O. Ikkala and R.H.A. Ras, Mechanically Durable Superhydrophobic Surfaces, *Adv. Mater.*, 2011, **23**(5), p 673-678.

21. L.R.J. Scarratt, U. Steiner and C. Neto, A Review on the Mechanical and Thermodynamic Robustness of Superhydrophobic Surfaces, *Adv. Coll. Interface. Sci.*, 2017, **246**, p 133-152. https://doi.org/10.1016/j.cis.2017.05.018

22. J.W. Song and L.W. Fan, Temperature Dependence of the Contact Angle of Water: A Review of Research Progress, Theoretical Understanding, and Implications for Boiling Heat Transfer, *Adv. Coll. Interface Sci.*, 2021, **288**, p 102339. https://doi.org/10.1016/j.cis.2020.102339

23. S. Barthwal, Y.S. Kim and S.-H. Lim, Mechanically Robust Superamphiphobic Aluminum Surface with Nanopore-Embedded Microtexture, *Langmuir*, 2013, **29**(38), p 11966-11974. https://doi.org/10.1021/la402600h

24. M. Ostapiuk, B. Surowska and J. Bieniaś, Interface Analysis of Fiber Metal Laminates, *Compos. Interface.*, 2014, **21**(4), p 309-318. https://doi.org/10.1080/15685543.2014.854527

25. H. Koivuluoto, A Review of Thermally Sprayed Polymer Coatings, *J. Therm. Spray Technol.*, 2022 https://doi.org/10.1007/s11666-022-01404-1

26. X. Chen, Y. Gong, D. Li and H. Li, Robust and Easy-Repairable Superhydrophobic Surfaces with Multiple Length-Scale Topography Constructed by Thermal Spray Route, *Coll. Surf. A Physicochem. Eng. Asp.*, 2016, **492**, p 19-25. https://doi.org/10.1016/j.colsurfa.2015.12.017

27. N. Sharifi, F. Ben Ettouil, C. Moreau, A. Dolatabadi and M. Pugh, Engineering Surface Texture and Hierarchical Morphology of Suspension Plasma Sprayed TiO2 Coatings to Control Wetting Behavior and Superhydrophobic Properties, *Surf. Coating. Technol.*, 2017, **329**, p 139-148.

28. P. Komarov, D. Jech, S. Tkachenko, K. Slámečka, K. Dvořák and L. Čelko, Wetting Behavior of Wear-Resistant WC-Co-Cr Cermet Coatings Produced by HVOF: The Role of Chemical Composition and Surface Roughness, *J. Therm. Spray Technol.*, 2021, **30**(1-2), p 285-303.

29. H. Koivuluoto, E. Hartikainen and H. Niemelä-Anttonen, Thermally Sprayed Coatings: Novel Surface Engineering Strategy towards Icephobic Solutions, *Materials*, 2020, **13**(6), p 1434.

30. T. Forati, N. Sharifi, T. Kaydanova, F. Ben Ettouil, N. Moghimian, M. Pugh, A. Dolatabadi and C. Moreau, Wetting and Corrosion Characteristics of Thermally Sprayed Copper-Graphene Nanoplatelet Coatings for Enhanced Dropwise Condensation Application, *Carbon Trend.*, 2021, **3**, p 1000. https://doi.org/10.1016/j.cartre.2020.100018

31. F.L. Toma, S. Alamri, B. Leupolt, T. Kunze and M. Barbosa, Functionalization of Suspension Sprayed HVOF TiO2 Coatings by Direct Laser Interference Patterning, *J. Therm. Spray Technol.*, 2021, **30**(5), p 1159-1173. https://doi.org/10.1007/s11666-021-01181-3

32. V. Donadei, H. Koivuluoto, E. Sarlin and P. Vuoristo, Lubricated Icephobic Coatings Prepared by Flame Spraying with Hybrid Feedstock Injection, *Surf. Coating. Technol.*, 2020, **403**, p 126396. https://doi.org/10.1016/j.surfcoat.2020.126396

33. M. Bai, H. Kazi, X. Zhang, J. Liu and T. Hussain, Robust Hydrophobic Surfaces from Suspension HVOF Thermal Sprayed Rare-Earth Oxide Ceramics Coatings, *Sci. Rep.*, 2018, **8**(1), p 1-8. https://doi.org/10.1038/s41598-018-25375-y

34. P. Xu, L. Pershin, J. Mostaghimi and T.W. Coyle, Efficient One-Step Fabrication of Ceramic Superhydrophobic Coatings by Solution Precursor Plasma Spray, *Mater. Lett.*, 2018, **211**, p 24-27. https://doi.org/10.1016/j.matlet.2017.09.077

35. H. Assadi, H. Kreye, F. Gärtner and T. Klassen, Cold Spraying—A Materials Perspective, *Acta Mater.*, 2016, **116**, p 382-407. https://doi.org/10.1016/j.actamat.2016.06.034

36. H. Koivuluoto and P. Vuoristo, Effect of Ceramic Particles on Properties of Cold-Sprayed Ni-20Cr+Al2O3 Coatings, *J. Therm. Spray Technol.*, 2009, **18**(4), p 555-562. https://doi.org/10.1007/s11666-009-9345-y

37. L. He and M. Hassani, A Review of the Mechanical and Tribological Behavior of Cold Spray Metal Matrix Composites, *J. Therm. Spray Technol.*, 2020 https://doi.org/10.1007/s11666-020-01091-w

38. R. Nikbakht, H. Assadi, K. Jahani, M. Saadati and B. Jodoin, Cold Spray Deformation and Deposition of Blended Feedstock Powders Not Necessarily Obey the Rule of Mixture, *Surf. Coatings Technol.*, 2021, **424**, p 127644. https://doi.org/10.1016/j.surfcoat.2021.127644

39. V. Champagne and D. Helfritch, Critical Assessment 11: Structural Repairs by Cold Spray, *Mater. Sci. Technol.*, 2015, **31**(6), p 627-634.

40. C.A. Widener, O.C. Ozdemir and M. Carter, Structural Repair Using Cold Spray Technology for Enhanced Sustainability of High Value Assets, *Proced. Manuf.*, 2018, **21**, p 361-368. https://doi.org/10.1016/j.promfg.2018.02.132

41. S. Eshkabilov, I. Ara, I. Sevostianov, F. Azarmi and X. Tangpong, Mechanical and Thermal Properties of Stainless Steel Parts, Manufactured by Various Technologies, in Relation to Their Microstructure, *Int. J. Eng. Sci.*, 2021, **159**, p 103398. https://doi.org/10.1016/j.ijengsci.2020.103398

42. J. Li, Y. Zhang, K. Ma, X. De Pan, C.X. Li, G.J. Yang and C.J. Li, Microstructure and Transparent Super-Hydrophobic Performance of Vacuum Cold-Sprayed Al2O3 and SiO2 Aerogel Composite Coating, *J. Therm. Spray Technol.*, 2018, **27**(3), p 471-482. https://doi.org/10.1007/s11666-017-0677-8

43. W. Lock Sulen, K. Ravi, C. Bernard, Y. Ichikawa and K. Ogawa, Deposition Mechanism Analysis of Cold-Sprayed Fluoropolymer Coatings and Its Wettability Evaluation, *J. Therm. Spray Technol.*, 2020, **29**(7), p 1643-1659. https://doi.org/10.1007/s11666-020-01059-w

44. H. Koivuluoto, J. Larjo, D. Marini, G. Pulci and F. Marra, Cold-Sprayed Al6061 Coatings: Online Spray Monitoring and Influence of Process Parameters on Coating Properties, *Coatings*, 2020, **10**(4), p 348.

45. J. Long, M. Zhong, H. Zhang and P. Fan, Superhydrophilicity to Superhydrophobicity Transition of Picosecond Laser Microstructured Aluminum in Ambient Air, *J. Coll. Interface Sci.*, 2015, **441**, p 1-9. https://doi.org/10.1016/j.jcis.2014.11.015

46. H.R. Sharma, M. Shimoda and A.P. Tsai, Quasicrystal Surfaces: Structure and Growth of Atomic Overlayers, *Adv. Phys.*, 2017, **56**(3), p 403-464.

47. K. Lee, J. Hsu, D. Naugle and H. Liang, Multi-Phase Quasicrystalline Alloys for Superior Wear Resistance, *Mater. Des.*, 2016, **108**, p 440-447. https://doi.org/10.1016/j.matdes.2016.06.113

48. T.P. Yadav and N.K. Mukhopadhyay, Quasicrystal: A Low-Frictional Novel Material, *Curr. Opin. Chem. Eng.*, 2018, **19**, p 163-169. https://doi.org/10.1016/j.coche.2018.03.005

49. C.J. Jenks and P.A. Thiel, Quasicrystals: A Short Review from a Surface Science Perspective, *Langmuir*, 1998, **14**(6), p 1392-1397.

50. J.M. Dubois and E. Belin-Ferré, Wetting and Adhesion Properties of Quasicrystals and Complex Metallic Alloys, *Appl Adhes Sci*, 2015 https://doi.org/10.1186/s40563-015-0046-0

51. J. Kong, C. Zhou, S. Gong and H. Xu, Low-Pressure Plasma-Sprayed Al-Cu-Fe-Cr Quasicrystalline Coating for Ti-Based Alloy Oxidation Protection, *Surf. Coatings Technol.*, 2003, **165**(3), p 281-285.

52. A.V. Byakova, M.M. Kiz, A.I. Sirko, M.S. Yakovleva and Y.V. Milman, Cold-Sprayed Coatings Based on High Strength Aluminium Alloys Reinforced by Quasicrystalline Particles: Microstructure and Key Properties, *High Temp. Mater. Process.*, 2010, **29**(5-6), p 325-337.

53. W. Wolf, C. Bolfarini, C.S. Kiminami and W.J. Botta, Recent Developments on Fabrication of Al-matrix Composites Reinforced with Quasicrystals: From Metastable to Conventional Processing, *J. Mater. Res.*, 2021, **36**(1), p 281-297. https://doi.org/10.1557/s43578-020-00083-4

54. N.W. Khun, R.T. Li, K. Loke and K.A. Khor, Effects of Al-Cr-Fe Quasicrystal Content on Tribological Properties of Cold-Sprayed Titanium Composite Coatings, *Tribol. Trans.*, 2015, **58**(4), p 616-624.

55. T.J. Watson, A. Nardi, A.T. Ernst, I. Cernatescu, B.A. Bedard and M. Aindow, Cold Spray Deposition of an Icosahedral-Phase-Strengthened Aluminum Alloy Coating, *Surf. Coatings Technol.*, 2017, **324**, p 57-63. https://doi.org/10.1016/j.surfcoat.2017.05.049

56. X. Guo, G. Zhang, W. Li, Y. Gao, H. Liao and C. Coddet, Investigation of the Microstructure and Tribological Behavior of Cold-Sprayed Tin-Bronze-Based Composite Coatings, *Appl. Surf. Sci.*, 2009, **255**(6), p 3822-3828. https://doi.org/10.1016/j.apsusc.2008.10.041

57. H. Koivuluoto, V. Matikainen, J. Larjo and P. Vuoristo, Novel Online Diagnostic Analysis for In-Flight Particle Properties in Cold Spraying, *J. Therm. Spray Technol.*, 2018, **27**(3), p 423-432. https://doi.org/10.1007/s11666-018-0685-3

58. S. Jithin, U.V. Bhandarkar and S.S. Joshi, Three-Dimensional Topography Analysis of Electrical Discharge Textured SS304

Surfaces, *J. Manuf. Process.*, 2020, **60**, p 384-399. https://doi.org/10.1016/j.jmapro.2020.10.066

59. N. Miyazaki, Solid Particle Erosion of Composite Materials: A Critical Review, *J. Compos. Mater.*, 2016, **50**, p 3175-3217.

60. W. Tillmann, L. Hagen, C. Schaak, J. Liß, M. Schaper, K.P. Hoyer, M.E. Aydinöz and K.U. Garthe, Adhesion of HVOF-Sprayed WC-Co Coatings on 316L Substrates Processed by SLM, *J. Therm. Spray Technol.*, 2020, **29**(6), p 1396-1409.

61. Y. Yamazaki, M. Arai, Y. Miyashita, H. Waki and M. Suzuki, Determination of Interfacial Fracture Toughness of Thermal Spray Coatings by Indentation, *J. Therm. Spray Technol.*, 2013, **22**(8), p 1358-1365.

62. S. Yin, M. Hassani, Q. Xie and R. Lupoi, Unravelling the Deposition Mechanism of Brittle Particles in Metal Matrix Composites Fabricated via Cold Spray Additive Manufacturing, *Scr. Mater.*, 2021, **194**, p 113614. https://doi.org/10.1016/j.scriptamat.2020.10.055

63. S. Wear, C. Al, and C. Al O, Comparative Study on the Cavitation Erosion And, 2020.

64. P. Pawlus, R. Reizer and M. Wieczorowski, Functional Importance of Surface Texture Parameters, *Materials (Basel)*, 2021, **14**(18), p 1-29.

65. Z. Zhu, S. Lou and C. Majewski, Characterisation and Correlation of Areal Surface Texture with Processing Parameters and Porosity of High Speed Sintered Parts, *Addit. Manuf.*, 2020, **36**, p 101402. https://doi.org/10.1016/j.addma.2020.101402

66. M. Yu, W.-Y. Li, X.K. Suo and H.L. Liao, Effects of Gas Temperature and Ceramic Particle Content on Microstructure and Microhardness of Cold Sprayed SiCp/Al 5056 Composite Coatings, *Surf. Coatings Technol.*, 2013, **220**, p 102-106. https://doi.org/10.1016/j.surfcoat.2012.05.050

67. N. Fan, J. Cizek, C. Huang, X. Xie, Z. Chlup, R. Jenkins, R. Lupoi and S. Yin, A New Strategy for Strengthening Additively Manufactured Cold Spray Deposits through In-Process Densification, *Addit. Manuf.*, 2020, **36**, p 101626. https://doi.org/10.1016/j.addma.2020.101626

68. N.D. Patil, R. Bhardwaj and A. Sharma, Droplet Impact Dynamics on Micropillared Hydrophobic Surfaces, *Exp. Therm. Fluid Sci.*, 2016, **74**, p 195-206. https://doi.org/10.1016/j.expthermflusci.2015.12.006

69. Hu. Jian, Q. Gu, Q. Guo, Y. Fan, L. Yang, C. Lv, C. Mai, Y. Jiang and H. Zhang, Preparation of the Pincushion-Like Multilayer Structure Materials by Amphiphilic Polymer for Biomimetic Super-Hydrophobic Materials, *Polym. Sci. - Ser. B*, 2022, **64**(2), p 161-175.

70. R. Jafari and E. Sadeghi, High-Temperature Corrosion Performance of HVAF-Sprayed NiCr, NiAl, and NiCrAlY Coatings with Alkali Sulfate/Chloride Exposed to Ambient Air, *Corros. Sci.*, 2019 https://doi.org/10.1016/j.corsci.2019.06.021

71. M.R. Rokni, C.A. Widener and V.R. Champagne, Microstructural Evolution of 6061 Aluminum Gas-Atomized Powder and High-Pressure Cold-Sprayed Deposition, *J. Therm. Spray Technol.*, 2014, **23**(3), p 514-524.

72. A.W.Y. Tan, J.Y. Lek, W. Sun, A. Bhowmik, I. Marinescu, P.J. Buenconsejo, Z. Dong and E. Liu, Microstructure, Mechanical and Tribological Properties of Cold Sprayed Ti6Al4V–CoCr Composite Coatings, *Compos. Part B Eng.*, 2020, **202**, p 108280. https://doi.org/10.1016/j.compositesb.2020.108280

73. V.N.V. Munagala, T.B. Torgerson, T.W. Scharf and R.R. Chromik, High Temperature Friction and Wear Behavior of Cold-Sprayed Ti6Al4V and Ti6Al4V-TiC Composite Coatings, *Wear*, 2019, **426-427**, p 357-369. https://doi.org/10.1016/j.wear.2018.11.032

74. W. Li, H. Assadi, F. Gaertner and S. Yin, A Review of Advanced Composite and Nanostructured Coatings by Solid-State Cold Spraying Process, *Crit. Rev. Solid State Mater. Sci.*, 2019, **44**(2), p 109-156. https://doi.org/10.1080/10408436.2017.1410778

75. R.N. Wenzel, Resistance of Solid Surfaces to Wetting by Water, *Ind. Eng. Chem.*, 1936, **28**(8), p 988-994. https://doi.org/10.1021/ie50320a024

76. A.B.D. Cassie and S. Baxter, Wettability of Porous Surfaces, *Trans. Faraday Soc.*, 1944, **40**, p 546. https://doi.org/10.1039/tf9444000546

77. H.Y. Erbil, The Debate on the Dependence of Apparent Contact Angles on Drop Contact Area or Three-Phase Contact Line: A Review, *Surf. Sci. Rep.*, 2014, **69**(4), p 325-365. https://doi.org/10.1016/j.surfrep.2014.09.001

78. J. Gao, Y. Wu, Z. Zhang, D. Zhao, H. Zhu, K. Xu and Y. Liu, Achieving Amorphous Micro-Nano Superhydrophobic Structures on Quartz Glass with a PTFE Coating by Laser Back Ablation, *Opt. Laser Technol.*, 2022, **149**, p 107927. https://doi.org/10.1016/j.optlastec.2022.107927

79. H. Koivuluoto, M. Kylmälahti, and P. Vuoristo, "Properties of Low-Pressure Cold-Sprayed Coatings for Repairing of Casting Defects," *International Thermal Spray Conference & Exposition (ITSC 2011)*, (Dusseldorf), DVS Media GmbH, 2011, p 1-6.

80. E. Huovinen, J. Hirvi, M. Suvanto and T.A. Pakkanen, Micro-Micro Hierarchy Replacing Micro-Nano Hierarchy: A Precisely Controlled Way to Produce Wear-Resistant Superhydrophobic Polymer Surfaces, *Langmuir*, 2012, **28**(41), p 14747-14755.

81. T. Peat, A. Galloway, A. Toumpis, P. McNutt and N. Iqbal, The Erosion Performance of Particle Reinforced Metal Matrix Composite Coatings Produced by Co-Deposition Cold Gas Dynamic Spraying, *Appl. Surf. Sci.*, 2017, **396**, p 1623-1634. https://doi.org/10.1016/j.apsusc.2016.10.155

82. R. Jafari, J. Kiilakoski, M. Honkanen, M. Vippola, and H. Koivuluoto, "Microstructure and Wetting Performance of High-Pressure Cold Sprayed Quasi-Crystalline Composite Coatings," *International Thermal Spray Conference*, 2022, p 63-71.